Aggregation behavior of the blends of PS-b-PEO-b-PS and PS-b-PMMA at the air/water interface

ARTICLE *in* RSC ADVANCES · SEPTEMBER 2014

Impact Factor: 3.84 · DOI: 10.1039/C4RA08579E

5 AUTHORS, INCLUDING:

Gangyao Wen
Harbin University of Science and Technology
14 PUBLICATIONS **80** CITATIONS
SEE PROFILE

Zhuang Wang
Harbin Institute of Technology
4 PUBLICATIONS **7** CITATIONS
SEE PROFILE

RSC Advances

PAPER

Cite this: *RSC Adv.*, 2014, **4**, 49219

Aggregation behavior of the blends of PS-*b*-PEO-*b*-PS and PS-*b*-PMMA at the air/water interface†

Xiaoqun Wang,[a] Gangyao Wen,*[a] Changchun Huang,[a] Zhuang Wang[a] and Yunbo Shi[b]

In order to explore the aggregation mechanisms of mixed polymeric Langmuir monolayers and enrich the structures of their corresponding Langmuir–Blodgett (LB) films, a predominantly hydrophilic triblock copolymer polystyrene-*block*-poly(ethylene oxide)-*block*-polystyrene (SEOS69K, M_n = 69 000, 43.5 wt% PEO) was mixed with an amphiphilic diblock copolymer polystyrene-*block*-poly(methyl methacrylate) (SMMA34K, M_n = 33 500, 26.9 wt% PMMA). The Langmuir monolayers and LB films of SEOS69K, SMMA34K, and their blends were characterized by the Langmuir monolayer technique and tapping mode atomic force microscopy (AFM), respectively. The isotherms of the samples deviate to large areas with the increase of the SEOS69K content and exhibit pseudo-plateaus for the samples with above 80 wt% SEOS69K. The hysteresis degree of the mixed Langmuir monolayer with 80 wt% SEOS69K compressed up to 30 mN m^{-1} is significantly larger than that with 20 wt% SEOS69K, which can be interpreted by a reasonable schematic illustration combining the predominant PEO and the few PEO/PMMA chain entanglements in the former with the low mobility of PEO and PMMA blocks. The mixed LB films with 10 wt% SEOS69K transferred at different pressures exhibit mixed structures of circular micelles and rod-like aggregates. However, all the other mixed LB films only exhibit circular micelles composed of PS cores and mixed PEO/PMMA coronas. Upon compression, the large close-packed aggregates split into small ones with more uniform sizes, which shows that the addition of SEOS69K can really improve the structure homogeneity of the mixed LB films. Moreover, a very simple formula was deduced to transform the isotherm of a mixed Langmuir monolayer as a function of a certain copolymer molecule area or repeating unit area.

Received 13th August 2014
Accepted 29th September 2014

DOI: 10.1039/c4ra08579e

www.rsc.org/advances

Introduction

The microstructures of block copolymers have drawn much attention due to their great capability of self-assembly.[1–3] Meanwhile, the aggregation behavior of amphiphilic diblock copolymers at the air/water interface has been widely studied for the ability of forming various surface aggregates.[4–24] The most widely studied system of diblock copolymer self-assembly at the air/water interface is polystyrene-*block*-poly(ethylene oxide) (PS-*b*-PEO),[10–17] whose PS block is water-insoluble and surface-inactive, but PEO block is water-soluble and surface-active. The formation of PS-*b*-PEO surface aggregates has been shown to be a spontaneous process due to an interplay of attractive interaction between PEO and water and repulsive interaction between PS and water or PEO.[12,13] By means of adjusting the relative length of PS and PEO blocks, various aggregate morphologies such as dots (circular aggregates), spaghetti (rod-like aggregates), and continents (planar aggregates) were obtained.[11] Seo *et al.* studied the effects of temperature and molecular weight on the aggregation behavior of polystyrene-*block*-poly(methyl methacrylate) (PS-*b*-PMMA) with very high molecular weight and explained the formation of PS-*b*-PMMA micelles was compression induced.[18–20] Furthermore, Deschenes *et al.* studied the interfacial behavior of PEO-PS-PEO triblock copolymers with the hydrophobic middle block and hydrophilic terminal blocks, and proposed a flowerlike surface micelle model to explain the organization of the circular surface micelles.[25]

There are more and more work focus on the interfacial behaviors of polymer blends composed of two homopolymers,[26–30] a homopolymer and a block copolymer,[31–33] and two block copolymers.[34–38] Sasaki *et al.* studied the mixed Langmuir monolayers of PMMA and poly(*n*-nonyl acrylate) (PNA) and received a hierarchical phase separation which was completely reversible and a true thermodynamic transition.[26] Kawaguchi *et al.* studied the surface morphology of the mixed LB films of poly(vinyl acetate) (PVAc) and poly(methyl acrylate) (PMA).[30]

[a]*Department of Polymer Materials and Engineering, College of Materials Science and Engineering, Harbin University of Science and Technology, Harbin 150040, P. R. China. E-mail: gywen@hrbust.edu.cn*

[b]*Institute of Measurement and Communication, Harbin University of Science and Technology, Harbin 150080, P. R. China*

† Electronic supplementary information (ESI) available: All the π–*A* isotherms with good superposition. Hysteresis curves of all the mixed Langmuir monolayers. Fig. 1 redrawn as a function of the mmA of SEOS69K. See DOI: 10.1039/c4ra08579e

They found that the surface images changed from granule islands to a Swiss cheese-like pattern with the increase of the PMA content, whereas the height and the number of granules increased with the increase of the PVAc content.

We once found a composition window for the mixed LB films of PS and polystyrene-*block*-poly(2-vinylpyridine) (PS-*b*-P2VP) to form necklace-network structures which were further controlled by adjusting spreading solution concentration and volume, subphase temperature, and transfer pressure.[31,32] Lopes *et al.* studied the interfacial behavior of the blends of PS and poly(isoprene-*b*-methyl methacrylate) (PI-*b*-PMMA), and found that the glassy globules of PS became softer in the presence of PI.[33]

In the mixed LB films of PS-*b*-P2VP and polystyrene-*block*-poly(ferrocenyl silane) (PS-*b*-PF), Seo *et al.* found that the morphology is predominantly spherical at low pressures, while it is transformed into a dense network of 'wires' at 11 mN m^{-1}.[34] Chung *et al.* studied the mixed surface micelles of PS-*b*-P2VP and PS-*b*-PMMA by premixed or separated spreading, and found that surface micelles sharing a PS core and mixed corona of P2VP and PMMA existed by premixed spreading, and independent PS-*b*-P2VP micelles and PS-*b*-PMMA micelles coexisted by separated spreading.[37] More recently, we performed an interesting way to control progressive morphology evolution in the mixed LB films of PS-*b*-PEO/PS-*b*-PMMA by mainly using a selective spreading solvent.[38]

In order to further explore the aggregation mechanisms of the mixed polymeric Langmuir monolayers and enrich the structures of their corresponding LB films, a predominantly hydrophilic triblock copolymer PS-*b*-PEO-*b*-PS with the hydrophilic middle block PEO and hydrophobic terminal blocks PS was chosen to mix with an amphiphilic diblock copolymer PS-*b*-PMMA. As far as we know, no work on the LB films of neat PS-*b*-PEO-*b*-PS and its corresponding blends was reported. We think the interfacial behavior of PS-*b*-PEO-*b*-PS and its corresponding blends may be different from those containing the amphiphilic diblock copolymers PS-*b*-PEO due to the looped PEO block in the former. In this work, the aggregation behavior of the Langmuir monolayers and the morphology of the LB films of PS-*b*-PEO-*b*-PS, PS-*b*-PMMA, and their blends were studied by the Langmuir monolayer technique and atomic force microscopy (AFM), respectively.

Experimental section

Materials

A predominantly hydrophilic triblock copolymer PS-*b*-PEO-*b*-PS with the hydrophilic middle block and hydrophobic terminal blocks (SEOS69K, M_w/M_n = 1.03, M_n of the three blocks are 19 500, 30 000, and 19 500, respectively, 43.5 wt% PEO), and an amphiphilic diblock copolymer PS-*b*-PMMA (SMMA34K, M_w/M_n = 1.07, M_n(PS) = 24 500, M_n(PMMA) = 9 000, 26.9 wt% PMMA) were purchased from Polymer Source Inc. (Canada) and used as received.

Preparation of the spreading solutions

Spreading solutions (0.50 mg mL^{-1}) of neat SEOS69K and neat SMMA34K were prepared with the nonselective solvent chloroform (HPLC grade). The mixed spreading solutions were further prepared by mixing the neat solutions of SEOS69K and SMMA34K at different volume ratios, which were coded as SEOS69K-wt% according to the weight fraction of SEOS69K, *i.e.*, SEOS69K-10%, SEOS69K-20%, SEOS69K-40%, SEOS69K-60%, and SEOS69K-80%, respectively. The spreading solutions were stored in a refrigerator and used within a week to avoid the concentration variation.

π–A experiments

A KSV Minitrough (Finland) with an effective trough area of 350 × 75 mm^2 was used to characterize the surface pressure–area (π–A) isotherms of the Langmuir monolayers of SEOS69K, SMMA34K, and their blends. The subphase water (resistivity of 18.25 MΩ cm) used in these experiments was purified and deionized after passing through the water purification system (Molecular 1810C, China). The surface pressure measurements were performed with a Wilhelmy plate, and subphase temperature was maintained at 25 ± 0.1 °C using a water bath (THD-0510, China) in all the experiments. The spreading solutions were carefully deposited on the water surface with a gastight Hamilton mini-syringe as well distributed as possible. All the spreading solution volumes were 20 μL except for neat SEOS69K (18.3 μL). The Langmuir monolayer was compressed symmetrically with two barriers whose relative speed was 10 mm min^{-1} after a 15 min period was allowed for the solvent to evaporate completely. All the isotherms were run for at least two or three times to obtain their superposed curves by precisely controlling the experimental conditions such as solution concentration, water level and temperature, homogeneous deposition, and dust-free environment, *etc.* (see ESI, Fig. S1–S6†).

The condition in the hysteresis (compression–expansion) experiments was similar to that of π–A isotherm experiments.[22] When surface pressure reached the maximum value (π_{max}), the barriers were stopped and kept for 30 s to allow the Langmuir monolayer to relax. After the expansion was completed, the barriers were kept still for 15 min, and then the procedure was repeated at the higher π_{max}.

Preparation of the LB films

The KSV Minitrough was also used to transfer the Langmuir monolayers onto silicon wafers to obtain the corresponding LB films under different surface pressures. Prior to the transfer, the silicon wafers were pretreated to be hydrophilic by mainly using a mixture of deionized water, ammonia–water, and hydroperoxide (5 : 1 : 1 in volume), and a mixture of deionized water, hydrochloric acid, and hydroperoxide (6 : 1 : 1 in volume) according to the procedure described in our previous paper.[32] Surface pressure was maintained for at least 20 min to obtain a stable monolayer, and then an LB film was prepared by vertically withdrawing a silicon wafer through the monolayer at a speed of 2 mm min^{-1}.

AFM measurements

The morphology of the LB films was characterized with a tapping mode AFM (SPA-300, Seiko Instruments Inc., Japan).

The spring constant of the cantilevers was 40 N m^{-1}. The scan areas and speeds in the AFM measurements were usually 2 μm × 2 μm and about 1.0 Hz, respectively. For an LB film, the AFM images were usually taken two or three times and far from the edges to make sure of good reproducibility.

Results and discussion

Isotherms

Fig. 1 shows the π–A isotherms of the Langmuir monolayers of SEOS69K, SMMA34K, and their blends at 25 °C. From Fig. 1, it can be seen that the isotherms deviate to large areas with the increase of the SEOS69K content. The isotherm of SMMA34K is featureless and surface pressure increases steeply after the onset pressure, which means the short hydrophilic PMMA blocks do not nearly contribute to surface pressure during the compression process. The isotherms of SEOS69K-20% to SEOS69K-60% are also featureless but surface pressure increases gradually after the onset pressure due to the contribution of PEO blocks, and then an inflexion occurs at about 12 mN m^{-1}. However, both of the isotherms of SEOS69K-80% and neat SEOS69K exhibit three regions, *i.e.*, pancake, pseudo-plateau, and brush regions. The pseudo-plateau region at about 10 mN m^{-1} is corresponding to the pancake-to-brush transition for overlapping PEO blocks upon compression.[14] Table 1 lists some important parameters obtained from Fig. 1. A_{ini} and π_{ini} represent the initial mean molecular area (mmA) and surface pressure prior to the compression, respectively. $A_{0,p}$ and $A_{0,b}$ represent the limiting mmA of the pancake and brush conformations, respectively.[15] With the increase of the SEOS69K content, from Table 1, it can be seen that all the values of A_{ini}, π_{ini}, and $A_{0,p}$ increase gradually due to the contribution of PEO blocks, and $A_{0,b}$ also increases in a slightly stepwise fashion with the decrease of the total PS content derived from SEOS69K and SMMA34K. Furthermore, the $A_{0,p}$ of SEOS69K (~25 $Å^2$ per EO unit) is slightly lower than those reported for diblock copolymers PS-*b*-PEO (27–31 $Å^2$)[11,14–16] with various compositions and significantly lower than those reported for PEO homopolymer (40–48 $Å^2$)[39] at the air/water interface, which means the stretching (or spreading) degree of PEO middle block in PS-*b*-PEO-*b*-PS at the air/water interface is slightly lower than that in PS-*b*-PEO but much lower than that in PEO homopolymer.

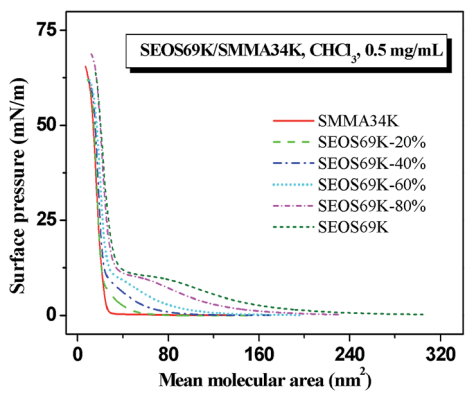

Fig. 1 π–A isotherms of the Langmuir monolayers of SEOS69K, SMMA34K, and their blends at 25 °C.

Hysteresis curves

Fig. 2 shows the hysteresis curves of neat SEOS69K and neat SMMA34K monolayers compressed to the different π_{max}. From Fig. 2, no hysteresis for the two samples are observed when the π_{max} reaches 10 mN m^{-1} and surface pressures finally return to their π_{ini} after the expansion process. The SEOS69K monolayer shows a large hysteresis loop when the π_{max} increases to 30 mN m^{-1} due to the pancake-to-brush transition. That is, the expansion curve drops sharply at the beginning, and then almost parallels to the compression curve below the pseudo-plateau, and finally surface pressure also returns to its π_{ini}, which is similar to those of amphiphilic diblock copolymers.[4,22] Hysteresis degree can be further quantified by $\Delta A_{0,p} = A_{0,p} - A'_{0,p}$ and $\Delta A_{0,b} = A_{0,b} - A'_{0,b}$, where $A'_{0,p}$ and $A'_{0,b}$ are the pancake and brush limiting areas in the expansion isotherm.[14] The values of $\Delta A_{0,p}$ and $\Delta A_{0,b}$ of SEOS69K are 2.30 and 17.44 nm^2, respectively, which indicates that a large hysteresis occurs and the highly compressed monolayer has undergone some rearrangement process whose kinetic barrier to return to the initial conformation is rather large.[15] That is, the re-adsorption of PEO brush at the air/water interface is much slower than the movement of the barriers due to the possible PEO chain entanglement and the low mobility of the looped PEO blocks, resulting in the rapid decay of surface pressure at the beginning of expansion. However, negligible hysteresis (ΔA_0 of 1.60 nm^2) for SMMA34K is observed when the π_{max} increases to 30 mN m^{-1} and finally surface pressure almost returns to its π_{ini}, which is much different from that spread with a selective solvent toluene.[38]

When the π_{max} is 10 mN m^{-1}, no hysteresis occur in the mixed Langmuir monolayers of SEOS69K-20% and SEOS69K-80%, and their hysteresis curves (see ESI, Fig. S7†) are similar to those of their neat components SMMA34K and SEOS69K, respectively. However, as shown in Fig. 3, obvious hysteresis occur in the monolayers of SEOS69K-20% and SEOS69K-80% compressed to the π_{max} = 30 mN m^{-1}, and the expansion isotherms cross their corresponding compression isotherms at 8.47 and 12.40 mN m^{-1}, and finally surface pressures remain at 1.65 and 5.35 mN m^{-1}, respectively. It is a little similar to the hysteresis curves of SMMA34K and the SEO19K/SMMA34K blends spread with toluene,[38] but quite different from those of neat SEOS69K (Fig. 2), amphiphilic diblock copolymers,[20,22] and polymer blends.[31,33] That is to say, the compression–expansion cycles of SEOS69K-20% and SEOS69K-80% are totally irreversible, which can also be seen in those of SEOS69K-40% and SEOS69K-60% (see ESI, Fig. S8†). The hysteresis degree of SEOS69K-80% ($|\Delta A_{0,p}|$ and $\Delta A_{0,b}$ of 73.27 and 11.62 nm^2, respectively) is much larger than those of SEOS69K-20% (5.71 and 3.45 nm^2) and SEO19K-20% (5.23 and 4.98 nm^2, ref. 38), which is also implied by their final surface pressures (5.35, 1.65, and 2.40 mN m^{-1}, respectively). The $|\Delta A_{0,p}|$ is the absolute value of $\Delta A_{0,p}$ due to the cross of the expansion isotherm through its

Table 1 Some important parameters obtained from Fig. 1[a]

Samples	SMMA34K	SEOS69K-20%	SEOS69K-40%	SEOS69K-60%	SEOS69K-80%	SEOS69K
A_{ini}[a] (nm^2)	139.16	149.33	170.18	195.51	226.70	304.24
π_{ini}[b] (mN m^{-1})	0.00	0.04	0.06	0.09	0.22	0.25
$A_{0,p}$[c] (nm^2)	—	48.63	67.33	88.84	135.85	172.14
$A_{0,b}$[d] (nm^2)	21.67	22.06	24.08	27.52	30.77	32.18

[a] Represents the initial mmA prior to the compression. [b] Represents the surface pressure prior to the compression. [c] Represents the limiting mmA of pancake, which is determined by extrapolating the linear region of 4–9 mN m^{-1} to the surface pressure of zero. [d] Represents the limiting mmA of brush, which is determined by extrapolating the steep linear region above 12 mN m^{-1} to the surface pressure of zero.

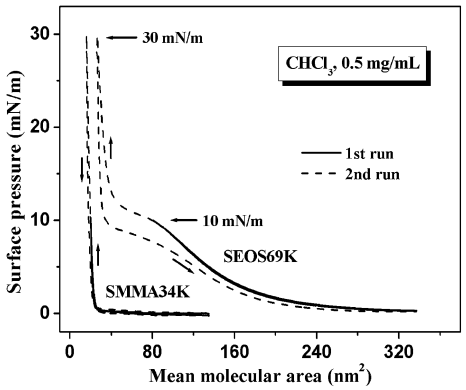

Fig. 2 Hysteresis curves of neat SEOS69K and neat SMMA34K monolayers. The π_{max} in the 1st and 2nd runs are 10 and 30 mN m^{-1}, respectively.

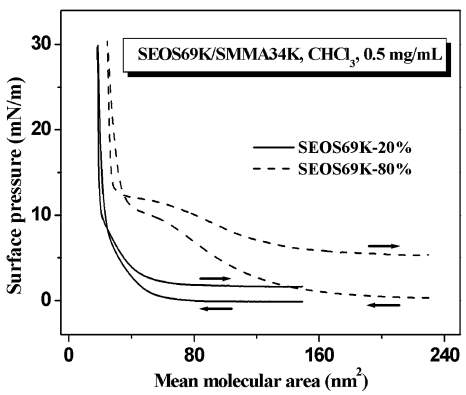

Fig. 3 Hysteresis curves of the mixed Langmuir monolayers of SEOS69K-20% and SEOS69K-80%. The π_{max} is 30 mN m^{-1}.

compression isotherm.[38] However, on the contrary, the hysteresis degree of the mixed SEO19K/SMMA34K monolayers with 80 wt% SEO19K is smaller than that with 20 wt% SEO19K,[38] which means the mobility of the free PEO blocks in PS-*b*-PEO is much higher than that of the looped PEO blocks in SEOS69K. Furthermore, the $|\Delta A_{0,p}|$ value of SEOS69K-80% (73.27 nm^2) is much larger than that of neat SEOS69K (2.30 nm^2), which indicates that the existence of PMMA blocks has a large effect on the rearrangement of PEO blocks. That is, besides of the predominant PEO chain entanglement, the few PEO/PMMA chain entanglement within the mixed micelle coronas also plays an important role. Upon expansion, the chain disentanglement in the mixed monolayer of SEOS69K-80% are much slower than those of SEOS69K-20% and SEO19K-80% (ref. 38) due to the strong PEO and PEO/PMMA chain entanglements and the low mobility of PEO and PMMA blocks in the former, finally resulting in the large hysteresis and the final surface pressure is well above its π_{ini}.

AFM images

In this section, AFM height images of the LB films of SEOE69K, SMMA34K, and their blends will be given in the following figures in which the bright domains represent the raised PS aggregates.[10,22,31,32] Fig. 4 shows the AFM height images of the LB films of neat SEOS69K transferred under different pressures at 25 °C. From Fig. 4, it can be seen that all the LB films of neat SEOS69K exhibit homogeneous circular micelles with very narrow distributions. Similar to diblock copolymer PS-*b*-PEO,[12] it is believed that the predominantly hydrophilic SEOS69K exists as random coils in the chloroform solution because chloroform is a good solvent for both blocks, and it tends to spontaneously form isolated circular micelles with PS cores and PEO coronas when the solution spreads on the water surface. Table 2 shows the statistical information of the nanoaggregates in Fig. 4. According to the AFM software, the data of root mean square (RMS) roughness and *Z* range can be directly obtained. In some AFM images with connected or close-packed aggregates, auto calculation of aggregate number by using the AFM software cannot reflect the real situations. Therefore, the aggregate number per μm^2 was counted by manual work, and average diameter was further evaluated with the total grain area obtained with the AFM software. Furthermore, average aggregation number (N_{agg})[6] of SEOS69K was calculated through dividing the area per aggregate by the mmA of SEOS69K at the corresponding transfer pressure (from its isotherm). Upon compression, according to Table 2, all the values of the average diameter (54–48 nm), RMS roughness (1.33–0.92 nm), and *Z* range (8–6 nm) of the PS aggregates decrease in a stepwise fashion, which is different from the pressure-independent aggregate sizes in the LB films of PS-*b*-PEO with 15.5–92 wt% PEO.[16] The N_{agg} of SEOS69K (29–39) increases upon compression due to the further aggregation, which is similar to diblock copolymers PS-*b*-P2VP.[22] The average diameter slightly decreases but the N_{agg} of SEOS69K significantly increases upon compression, together with the decreasing mmA values, which

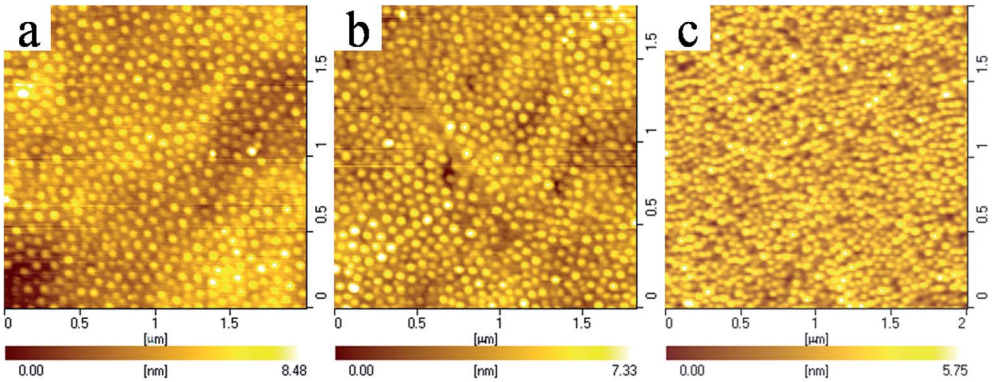

Fig. 4 AFM height images of the LB films of neat SEOS69K transferred at 25 °C. Transfer pressures: 0.5 (a), 2 (b), and 7 mN m^{-1} (c). Scan area: 2 μm × 2 μm.

Table 2 Statistical information of the nanoaggregates in Fig. 4[a]

Panels	a	b	c
Number per μm^2	138 ± 11	191 ± 4	254 ± 7
Diameter range (nm)	40–70	40–60	40–60
Average diameter (nm)	54 ± 1	49 ± 3	48 ± 1
RMS roughness[b] (nm)	1.33	1.14	0.92
mmA[c] (nm^2)	257.48	175.02	100.15
N_{agg}[d]	28 ± 2	30 ± 1	39 ± 1
Z range (nm)	8	7	6

[a] Standard deviations were induced from the analysis of different regions of the AFM images. [b] Represents the root mean square roughness of the nanoaggregates. [c] The values are given according to Fig. 1. [d] Represents the average aggregation number of SEOS69K, *i.e.*, average molecular number of SEOS69K per nanoaggregate.

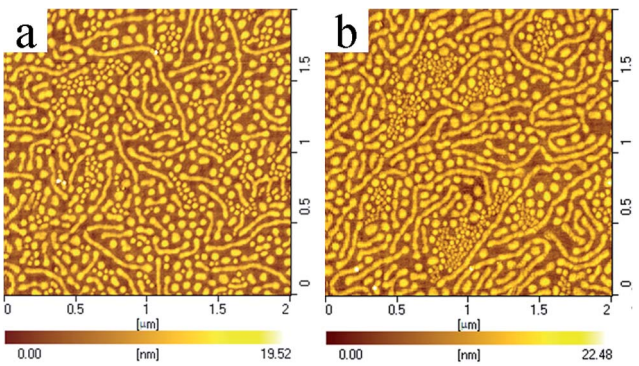

Fig. 5 AFM height images of the LB films of neat SMMA34K transferred at 25 °C. Transfer pressures: 0.2 (a) and 7 mN m^{-1} (b). Scan area: 2 μm × 2 μm.

indicates that the compactness of the aggregates become higher and higher. It is worth noting that Baker *et al.* found that the pressure-independent N_{agg} of predominantly hydrophilic PS-*b*-PEO was to be equal to 250 − 240 × (wt% PEO) (the value 240 used here instead of 2.4 in their original formula) for solutions ranged from 0.5 to 1.2 mg mL^{-1}.[16] Using this formula, the N_{agg} of our SEOS69K would be 146, which is significantly larger than our experimental values. It indicates that the aggregation degree of triblock copolymer PS-*b*-PEO-*b*-PS must be much lower than that of PS-*b*-PEO due to the low mobility of the looped PEO blocks in the former.

Fig. 5 shows the AFM height images of the LB films of neat SMMA34K transferred under different pressures at 25 °C. Both of panels a and b exhibit mixed structures of circular micelles and rod-like aggregates, but the predominant structures are circular micelles and rod-like aggregates, respectively. In panel a, the diameter and height of the typically large circular micelle cores are ~60 and 15 nm, and those of the typically small micelle cores and rod-like aggregates are both ~30 and 12 nm, respectively. It means that the rod-like aggregates are probably composed of small circular micelle cores. Upon compression (panel b), the diameter and height of the typically large circular micelle cores increase to ~70 and 18 nm, and those of the typically small micelle cores and the rod-like aggregates are still ~30 and 13 nm and increase to ~40 and 15 nm, respectively. SMMA34K with a relatively low molecular weight probably tends to spontaneously form the circular micelles composed of PS cores and PMMA coronas with the spread of its solution and the evaporation of solvent. Meanwhile, some circular micelle cores contact with each other and coalesce to the rod-like aggregates due to the relative short PMMA block (26.9 wt%), which can be deduced from their similar diameters. It is quite different from the formation of surface micelles *via* a compression-induced process for PS-*b*-PMMA with a very high molecular weight.[18,19] Upon compression, it appears some circular micelles tend to coalesce and the LB film exhibits more rod-like aggregates and large circular micelles, and the rest small micelles simply aggregate together in some regions without size variation due to the lack of enough compression (Fig. 5b).

Fig. 6 shows the AFM height images of the mixed LB films of SEOS69K/SMMA34K transferred under different pressures at 25 °C. From Fig. 6, it can be seen that the mixed LB films of SEOS69K-20% and SEOS69K-40% transferred at 0.5 mN m^{-1} already exhibit significantly close-packed circular aggregates, while those of SEOS69K-60% and SEOS69K-80% still exhibit some isolated circular micelles due to their relatively higher

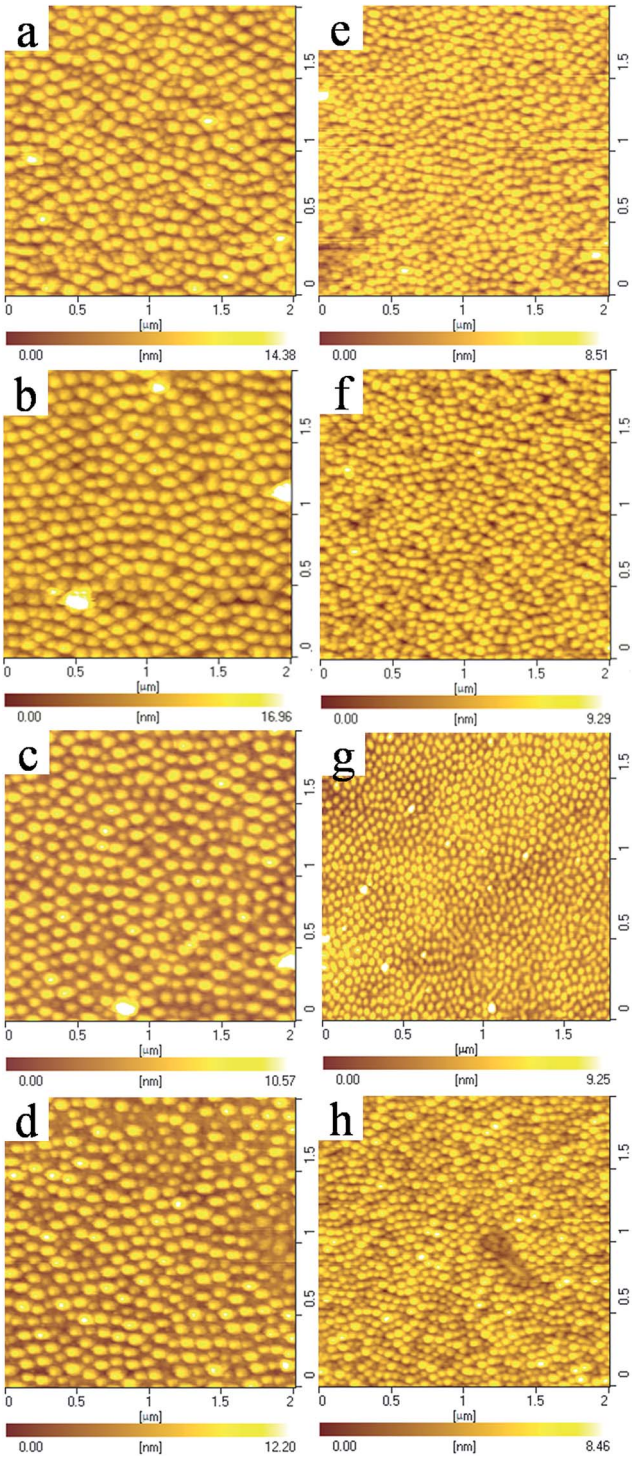

Fig. 6 AFM height images of the mixed LB films of SEOS69K/SMMA34K transferred at 25 °C. Samples: SEOS69K-20% (a and e), SEOS69K-40% (b and f), SEOS69K-60% (c and g), and SEOS69K-80% (d and h). Transfer pressures: 0.5 (a–d) and 7 mN m^{-1} (e–h). Scan area: 2 μm × 2 μm.

SEOS69K content. Similar to Tables 2 and 3 shows the statistical information of the nanoaggregates in Fig. 6. As for the calculation of N_{agg} of SEOS69K in the mixed LB films, mmA′ of SEOS69K, instead of mmA of the mixtures, cannot simply be obtained from Fig. 1, which needs to redraw the isotherms as a function of mmA′ of SEOS69K. In our opinion, M_n and mmA of a mixture calculated with Formulae (1) and (2) can be used to obtain the π–A isotherm of the mixed monolayer. No corresponding formulae were given in the manual of the KSV Minitrough and an isotherm was automatically obtained by just inputting the experimental parameters of M_n, spreading solution concentration, and deposition volume during the isothermal experiment.

$$M = 1/(w_1/M_1 + w_2/M_2) \quad (1)$$

$$\mathrm{mmA} = AM/(mN_0) \quad (2)$$

Here M, M_1, and M_2 represent the M_n of the mixture and its two components, respectively. Here w_1 and w_2 are the weight fractions of the two components. Here mmA and A represent the mean molecular area of the mixture and the real-time monolayer area, respectively. The parameters m and N_0 are the mass of the mixture and the Avogadro constant, respectively. Similarly, mmA′ of component 1 can be expressed as

$$\mathrm{mmA}' = AM_1/(m_1N_0) \quad (3)$$

Here m_1 represents the mass of component 1. Combining Formulae (2) and (3) with $w_1 = m_1/m$, it is easy to build the relationship between mmA′ and mmA as follows.

$$\mathrm{mmA}' = M_1/(Mw_1)\mathrm{mmA} \quad (4)$$

Therefore, it was very convenient for us to redraw the isotherms of the mixed monolayers as a function of mmA′ of SEOS69K with the Origin software by using Formula (4) (see ESI, Fig. S9†). Of course, this formula can also be used to transform the isotherm of a mixture (or copolymer) as a function of the repeating unit area (this moment, M_1 and w_1 represent the molecular weight and weight fraction of the corresponding repeating unit, respectively), which was also performed in our previous papers.[31,32]

According to Table 3, the average diameters of the aggregates in the mixed LB films (73–81 nm) with different compositions transferred at low pressure are larger than those in the neat SEOS69K (54 nm) and SMMA34K films (30–60 nm). While the heights of the aggregates in the mixed LB films (11–17 nm) are close to or larger than those in the neat SMMA34K (12–15 nm) and SEOS69K films (7 nm), respectively. Therefore, it can be deduced that the mixed LB films of SEOS69K/SMMA34K with 20–80 wt% SEOS69K exhibit the mixed circular micelles (aggregates) composed of PS cores and mixed PEO/PMMA coronas. Upon compression to 7 mN m^{-1}, all the mixed LB films (panels e–h) exhibit much more uniform (RMS roughness of 1.27–1.48 nm) close-packed aggregates with significantly smaller diameters (39–59 nm) and height (8–9 nm) compared with those transferred at 0.5 mN m^{-1}. The large close-packed aggregates transform (probably split) into small ones, which is different from the above simply compacted SEOS69K aggregates but some similar to our another blend system PS/PS-*b*-P2VP and

Table 3 Statistical information of the nanoaggregates in Fig. 6

Panels	a	b	c	d	e	f	g	h
Number per μm^2	100 ± 2	90 ± 2	89 ± 2	88 ± 4	198 ± 13	185 ± 8	359 ± 21	220 ± 18
Diameter range (nm)	60–160	70–130	60–120	50–120	50–80	50–70	35–50	40–80
Average diameter (nm)	77 ± 1	81 ± 3	73 ± 1	73 ± 1	57 ± 2	59 ± 2	39 ± 2	50 ± 2
RMS roughness (nm)	2.40	2.80	1.99	2.25	1.31	1.48	1.27	1.36
mmA′ of SEOS69K[a] (nm^2)	547.39	369.20	305.08	294.51	237.67	147.37	122.16	122.31
N_{agg} of SEOS69K	18 ± 1	30 ± 1	37 ± 1	39 ± 2	21 ± 1	37 ± 2	23 ± 1	37 ± 3
Z range (nm)	14	17	11	12	9	9	9	8

[a] According to the isotherms of the mixed Langmuir monolayers (Fig. 1) redrawn as a function of the mmA of SEOS69K (see ESI, Fig. S9†).

the barriers move back and forth for 20 min prior the transfer to provide the necessary power (or driving force) for the chain motion.[32] Furthermore, the N_{agg} of SEOS69K in the mixed LB films transferred at 0.5 mN m^{-1} increase with the increase of the SEOS69K content and are larger than that in the neat SEOS69K film due to their relatively low SEOS69K content. However, the N_{agg} of SEOS69K in the mixed LB films transferred at 7 mN m^{-1} are smaller than that in the neat SEOS69K film, which further supports the splitting interpretation instead of the compacting interpretation for the former.

It is worth noting that all of the mixed LB films with above 20 wt% SEOS69K do not exhibit the rod-like aggregates (like neat SMMA34K) due to the large content of the middle PEO block (43.5 wt% PEO) in SEOS69K. It is likely to question whether it is still possible for this mixed system to exhibit some rod-like aggregates when the SEOS69K content is low enough. In order to answer this question, the mixed LB films of SEOS69K-10% were further prepared and characterized by AFM. Fig. 7 shows the AFM height images of the mixed LB films of SEOS69K-10% transferred under different pressures at 25 °C. From Fig. 7, it can be seen that all the LB films of SEOS69K-10% exhibit mixed structures of circular micelles and rod-like aggregates which are much different from those of SMMA34K (see Fig. 5). In panel a, the diameter and height of the typically large circular micelle cores are ~60 and 10 nm, and those of the typically small micelle cores and rod-like aggregates are both ~40 and 6 nm, respectively. In panel b, the diameter and height of the typically large circular micelle cores are ~50 and 7 nm, and those of the typically small micelle cores and rod-like aggregates are both ~40 and 6 nm, respectively. Upon further compression, the LB film (panel c) exhibits a closed-packed mixed structure of predominant rod-like aggregates (~30 and 8 nm in diameter and height, respectively) and some uniform circular micelle cores (~40 and 9 nm). Compared with the LB films of neat SMMA34K, the mixed LB films are more likely to exhibit uniform structures due to the small amount addition of SEOS69K.

Possible surface aggregate evolutions in the mixed Langmuir monolayers

According to the hysteresis curves (Fig. 3) and AFM images (Fig. 6), the possible surface aggregate evolutions in the mixed Langmuir monolayers of SEOS69K-20% and SEOS69K-80% are considered. Fig. 8 shows the schematic illustration of the initial and the final states during the compression processes, and the final states during the expansion processes of SEOS69K-20% and SEOS69K-80% monolayers at the air/water interface. When the mixed solutions are deposited onto the water (panels a and d), PEO and PMMA blocks tend to spread out at the interface to form the mixed micelle coronas, but the stretching degree of the strongly hydrophilic PEO blocks is much larger than that of the weakly hydrophilic PMMA blocks. However, PS blocks tend to leave the water surface and form the micelle cores due to the

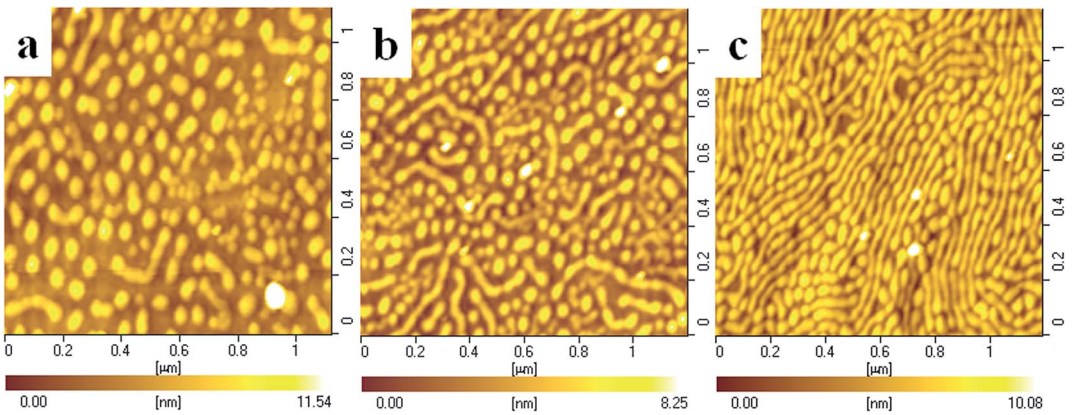

Fig. 7 AFM height images of the LB films of SEOS69K-10% transferred at 25 °C. Transfer pressures: 0.2 (a), 2 (b), and 7 mN m^{-1} (c).

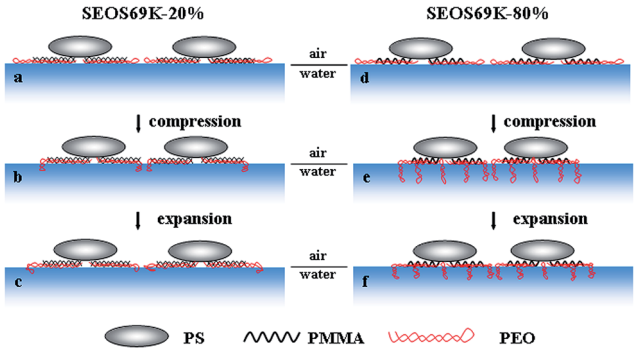

Fig. 8 Schematic illustration of the initial (a and d) and the final states (b and e) during the compression process, and the final states (c and f) during the expansion process of SEOS69K-20% (a–c) and SEOS69K-80% monolayers (d–f) at the air/water interface.

repulsion interactions between PS blocks and water or PEO blocks.[12,13]

Upon compression, it is possible for very short sections of the limited amount of the looped PEO blocks in SEOS69K-20% (block molar ratio, $n_{PMMA}/n_{PEO} = 8.2$) to submerge into water (panel b), which is consistent with the lack of a transition plateau in its monolayer compression isotherm (see Fig. 1). Furthermore, it is likely to form the predominant PEO/PMMA and the few PMMA chain entanglements within the SEOS69K-20% micelle coronas because the amount of MMA unit is slightly more than that of EO unit (unit molar ratio, $n_{MMA}/n_{EO} = 1.1$), and the LB films exhibit close-packed circular aggregates (like Fig. 6b). On the contrary, long sections of the relatively large amount of PEO blocks in SEOS69K-80% ($n_{PEO}/n_{PMMA} = 1.9$) are probably submerged into water upon compression (panel e), which is implied by its pseudo-plateau. It results in the predominant PEO and the few PEO/PMMA chain entanglements within the SEOS69K-80% micelle coronas because the amount of EO unit is much more than that of MMA unit ($n_{EO}/n_{MMA} = 14.7$), and the LB films exhibit the loose-packed circular aggregates (like Fig. 6d).

Upon expansion, the distance between the PS aggregates in the SEOS69K-20% monolayer will enlarge with a certain extension of the micelle coronas (panel c) due to the slow PEO/PMMA chain disentanglement, finally resulting in a relatively small hysteresis of SEOS69K-20% monolayer (see Fig. 3). However, only small parts of the immerged PEO sections of SEOS69K-80% can re-adsorb at the air/water interface (panel f) due to the compression-induced predominant PEO and few PEO/PMMA chain entanglements, and the low mobility of the looped PEO blocks and the PMMA blocks, which finally results in the large hysteresis of SEOS69K-80% monolayer (see Fig. 3).

Conclusions

In this paper, the Langmuir monolayers and LB films of SEOS69K, SMMA34K, and their blends were studied by the Langmuir monolayer technique and tapping mode AFM, respectively. The isotherms deviate to large areas with the increase of the SEOS69K content and exhibit pseudo-plateaus for the samples with above 80 wt% SEOS69K. The compression–expansion processes of SMMA34K at the low and high π_{max} are both reversible, while the SEOS69K monolayer shows an obvious hysteresis loop at the high π_{max} due to the pancake-to-brush transition. Furthermore, all the mixed Langmuir monolayers show hysteresis when the π_{max} is above the transitional plateau, and the final surface pressures do not return to their π_{ini}. The hysteresis degree of SEOS69K-80% is significantly larger than that of SEOS69K-20%, which can be interpreted by a reasonable schematic illustration combining the predominant PEO and the few PEO/PMMA chain entanglements in the former with the low mobility of PEO and PMMA blocks. According to the AFM images, neat SEOS69K and neat SMMA34K can spontaneously form the isolated circular micelles, and the mixed structure of predominantly circular micelles and some rod-like aggregates, respectively. However, all the mixed LB films of SEOS69K/SMMA34K (except for SEOS69K-10%) only exhibit the mixed circular aggregates composed of PS cores and mixed PEO/PMMA coronas. Upon compression, the large close-packed aggregates split into small ones with more uniform sizes, which shows that the addition of SEOS69K can really improve the structure homogeneity of the mixed LB films. Moreover, a very simple formula was deduced to transform the isotherm of a mixed Langmuir monolayer as a function of a certain copolymer molecule area or repeating unit area.

Acknowledgements

This work was supported by the open fund of "Heilongjiang Provincial Key Laboratory of Colleges and Universities of Material Research and Application (Harbin University of Science and Technology)".

References

1 M. S. Weiser, Y. Thomann, L. C. Heinz, H. Pasch and R. Mulhaupt, *Polymer*, 2006, **47**, 4505–4512.
2 C. Vasilev, G. Reiter, S. Pispas and N. Hadjichristidis, *Polymer*, 2006, **47**, 330–340.
3 D. Wang, H. Ma, C. Chu, J. Hao and H.-G. Liu, *J. Colloid Interface Sci.*, 2013, **402**, 75–85.
4 X. Wang, X. Ma and D. Zang, *Soft Matter*, 2013, **9**, 443–453.
5 T. J. Joncheray, K. M. Denoncourt, M. A. R. Meier, U. S. Schubert and R. S. Duran, *Langmuir*, 2007, **23**, 2423–2429.
6 J. Zhu, R. B. Lennox and A. Eisenberg, *Langmuir*, 1991, **7**, 1579–1584.
7 J. Zhu, A. Eisenberg and R. B. Lennox, *J. Am. Chem. Soc.*, 1991, **113**, 5583–5588.
8 J. Zhu, R. B. Lennox and A. Eisenberg, *J. Phys. Chem.*, 1992, **96**, 4727–4730.
9 P. C. D. Claro, M. E. Coustet, C. Diaz, E. Maza, M. S. Cortizo, F. G. Requejo, L. I. Pietrasanta, M. Ceolin and O. Azzaroni, *Soft Matter*, 2013, **9**, 10899–10912.
10 C. P. Glagola, L. M. Miceli, M. A. Milchak, E. H. Halle and J. L. Logan, *Langmuir*, 2012, **28**, 5048–5058.

11 C. A. Devereaux and S. M. Baker, *Macromolecules*, 2002, **35**, 1921–1927.
12 J. K. Cox, K. Yu, B. Constantine, A. Eisenberg and R. B. Lennox, *Langmuir*, 1999, **15**, 7714–7718.
13 R. B. Cheyne and M. G. Moffitt, *Langmuir*, 2005, **21**, 5453–5460.
14 R. B. Cheyne and M. G. Moffitt, *Langmuir*, 2006, **22**, 8387–8396.
15 A. M. Goncalves da Silva, E. J. M. Filipe, J. M. R. d'Oliveira and J. M. G. Martinho, *Langmuir*, 1996, **12**, 6547–6553.
16 S. M. Baker, K. A. Leach, C. E. Devereaux and D. E. Gragson, *Macromolecules*, 2000, **33**, 5432–5436.
17 A. M. Goncalves da Silva, A. L. Simoes Gamboa and J. M. G. Martinho, *Langmuir*, 1998, **14**, 5327–5330.
18 Y. Seo, K. Paeng and S. Park, *Macromolecules*, 2001, **34**, 8735–8744.
19 Y. Seo, J.-H. Im, J.-H. Lee and J.-H. Kim, *Macromolecules*, 2001, **34**, 4842–4851.
20 Y. Seo, C. Y. Cho, M. Hwangbo, H. J. Choi and S. M. Hong, *Langmuir*, 2008, **24**, 2381–2386.
21 B. Chung, M. Choi, M. Ree, C. Jin, C. Wang and T. Chang, *Macromolecules*, 2006, **39**, 684–689.
22 G. Wen, B. Chung and T. Chang, *Polymer*, 2006, **47**, 8575–8582.
23 M. Choi, B. Chung, B. Chun and T. Chang, *Macromol. Res.*, 2004, **12**, 127–133.
24 J. Zhang, H. Cao, X. Wan and Q. Zhou, *Langmuir*, 2006, **22**, 6587–6592.
25 L. Deschenes, M. Bousmina and A. M. Ritcey, *Langmuir*, 2008, **24**, 3699–3708.
26 Y. Sasaki, N. Aiba, H. Hashimoto and J. Kumaki, *Macromolecules*, 2010, **43**, 9077–9086.
27 S. Wu and J. R. Huntsberger, *J. Colloid Interface Sci.*, 1969, **29**, 138–147.
28 M. Kawaguchi and R. Nishida, *Langmuir*, 1990, **6**, 492–496.
29 G. Gabrielli, M. Puggelli and E. Ferroni, *J. Colloid Interface Sci.*, 1974, **47**, 145–154.
30 M. Kawaguchi, S. Suzuki, T. Imae and T. Kato, *Langmuir*, 1997, **13**, 3794–3799.
31 G. Wen, B. Chung and T. Chang, *Macromol. Rapid Commun.*, 2008, **29**, 1248–1253.
32 G. Wen, *J. Phys. Chem. B*, 2010, **114**, 3827–3832.
33 S. I. C. Lopes, A. M. P. S. Goncalves da Silva, P. Brogueira, S. Picarra and J. M. G. Martinho, *Langmuir*, 2007, **23**, 9310–9319.
34 Y. S. Seo, K. S. Kim, A. Galambos, R. G. H. Lammertink, G. J. Vancso, J. Sokolov and M. Rafailovich, *Nano Lett.*, 2004, **4**, 483–486.
35 D. Xie, C. A. Rezende, G. Liu, S. Pispas, G. Zhang and L.-T. Lee, *J. Phys. Chem. B*, 2009, **113**, 739–744.
36 E. W. Price, Y. Guo, C.-W. Wang and M. G. Moffitt, *Langmuir*, 2009, **25**, 6398–6406.
37 B. Chung, H. Choi, H.-W. Park, M. Ree, J. C. Jung, W. C. Zin and T. Chang, *Macromolecules*, 2008, **41**, 1760–1765.
38 Z. Wang, G. Wen, F. Zhao, C. Huang, X. Wang, T. Shi and H. Li, *RSC Adv.*, 2014, **4**, 29595–29603.
39 B. B. Sauer and H. Yu, *Macromolecules*, 1989, **22**, 786–791.